**Article:**

Mernild, S.H., Beckerman, A.P., Knudsen, N.T. et al. (2018) Statistical EOF analysis of spatiotemporal glacier mass-balance variability: a case study of Mittivakkat Gletscher, SE Greenland. Geografisk Tidsskrift-Danish Journal of Geography, 118 (1). pp. 1-16. ISSN: 0016-7223

https://doi.org/10.1080/00167223.2017.1386581

# Statistical EOF analysis of spatiotemporal glacier mass-balance variability: A case study of Mittivakkat Gletscher, SE Greenland


SEBASTIAN H. MERNILD

*Nansen Environmental and Remote Sensing Center, Bergen, NORWAY*
*Faculty of Engineering and Science, Western Norway University of Applied Science, Sogndal, NORWAY*
*Antarctic and Sub-Antarctic Program, Universidad de Magallanes, Punta Arenas, CHILE*

ANDREW P. BECKERMAN

*Department of Animal and Plant Sciences, University of Sheffield, UK*

NIELS TVIS KNUDSEN

*Department of Geoscience, Aarhus University, Aarhus, DENMARK*

BENT HASHOLT

*Department of Geosciences and Natural Resource Management, University of Copenhagen, DENMARK*

JACOB C. YDE

*Faculty of Engineering and Science, Western Norway University of Applied Science, Sogndal, NORWAY*



*Accepted Danish Journal of Geography, September 27, 2017*



Corresponding author address:
Dr. Scient. Sebastian H. Mernild
E-mail: sebastian.mernild@nersc.no

## Abstract

An Empirical Orthogonal Function (EOF) variance analysis was performed to map and elucidate in detail the spatiotemporal variability in individual stake mass-balances ($b_a$) on the Mittivakkat Gletscher (MG) – in a region where at present five out of ~20.000 glaciers have mass-balance observations. The EOF analysis suggested that observed $b_a$ was summarized by two major modes: EOF1 and EOF2 represented 80 % (significant) and 6 % (insignificant) of the explained variance, respectively. EOF1 captured a decline in $b_a$ that was uniformly distributed in space at all stakes. The decline was correlated with: 1) albedo observations; and 2) surface air temperature observations from nearby maritime and coastal stations. EOF2, however, described variations in $b_a$ that were heterogeneously distributed among stakes and associated with local slope and aspect. Low-elevation stakes (~<400 m a.s.l.) showed relatively negative (out of phase) correlation and higher elevated stakes relatively positive (in phase) eigenvector correlation values with EOF2. Such relatively negative and positive eigenvector correlation values were present where the surface of MG constituted of exposed glacier ice or snow cover, respectively. The results from this study show how EOF analyses can provide robust information on spatiotemporal patterns of glacier mass-balance. Understanding such detailed variabilities in mass-balance on a Greenlandic glacier is of interest because a fifth of the Arctic contribution from glaciers and ice caps to sea-level rise originated from Greenland.

**Keywords** Empirical Orthogonal Function analysis; Greenland; observations; mass-balance stakes; Mittivakkat Gletscher

## 1. Introduction

At present, glaciers and ice caps are important contributors to eustatic sea-level rise (e.g., Marzeion et al. 2012; Gardner et al. 2013; Allison et al. 2015). Over the last several decades, glaciers and ice caps in the Arctic have been observed to decrease in area and volume in response to climate changes contributing to sea-level changes (Leclercq et al. 2011; Bjørk et al. 2012; Cogley 2012; Kargel et al. 2012; Marzeion et al. 2012; Zemp et al. 2015). Direct glaciological surface mass-balance time series and glacier meteorology observations from local glaciers (i.e. glaciers and ice caps surrounding the continental ice sheets; Weidick and Morris 1998) are scarce and sparsely distributed in Greenland. In total, less than 20 local glaciers in Greenland have recorded mass-balance ($B_a$) observations covering different time periods since 1892-93 and to present (Machguth et al. 2016). At present, only five glaciers out of ~20,000 individual local glaciers in Greenland have ongoing annual glacier mass-balance observation programs. This is a minor fraction of local glaciers in Greenland (Pfeffer et al. 2014; Radić et al. 2014), which cover a total area of ~89,300 ± 2,800 km$^2$ (Rastner et al. 2012). This lack of glacier mass-balance observations leaves us with limited information about local glacier conditions in Greenland and its contribution to sea-level changes. Local glaciers in Greenland are, for example, less well-studied than the main ice sheet, so processes driving their change and their sensitivity to climate variables are more unclear. However, it was recently stated by AMAP (2017) that a fifth of the Arctic contribution from glaciers and ice caps to sea-level rise originates from Greenland. It is, therefore, important to extract and generalize all relevant information about these monitored glaciers.

Mittivakkat Gletscher (henceforth MG), located in Southeast Greenland on Ammassalik Island, is Greenland's *only* peripheral glacier for which there exist long-term ongoing $B_a$ records continuously since the mass-balance year 1995/96 (Mernild et al. 2011). Even before this time, B. Fristrup in 1933, 1958, and 1970 and B. Hasholt in 1986 and 1998 have demonstrated relationships between climate-induced surface ablation and $b_a$ variations and freshwater runoff on MG (Fristrup 1970; Hasholt and Jakobsen 2008). The four other local glaciers in Greenland with ongoing mass-balance monitoring programs are A. P. Olsen Iskappe (74.6°N, Zackenberg, East Greenland; Larsen et al. 2012), Freya Gletscher (74.4°N, Clavering Island, East Greenland; Hynek et al. 2014), Qaanaaq Gletscher, which is a part of Qaanaaq Iskappe (74.4°N, Qaanaaq, Northwest Greenland; Sugiyama et al. 2014), and Qassinnguit Gletscher (64.1°N, Nuuk/Kobberfjord, West Greenland; Abermann et al. 2014). The longest continuous observational program beside the MG mass-balance program goes back to 2007 and is operated by the Austrian Polar Research Institute on Freya Gletscher (Hynek et al. 2014; Machguth et al. 2016). A common characteristic for all ongoing local glacier mass-balance programs in Greenland is that they show mean negative $B_a$ for their period of observations.

As the MG mass-balance record started in 1995/96, MG is a valuable study site for obtaining detailed understanding of trends in mass-balance (for both $B_a$ and $b_a$) in Southeast Greenland. On catchment-scale, MG also serves as an important site for studying the variability of morphological characteristics (area, mean thickness, volume, surface slope, etc.) and ice dynamics (Mernild et al. 2013a) and the climate sensitivity of local glaciers in Greenland (Mernild et al. 2011, 2013b). Local glaciers in Southeast Greenland are influenced by air temperature and precipitation changes following the oscillation in the Atlantic Multidecadal Oscillation (AMO; Kaplan et al. 1998), where a relatively high temperature anomaly is in anti-phase with a relatively low precipitation anomaly (during positive AMO), and vice versa (during negative AMO) (Chylek et al. 2009; Mernild et al. 2012a). Since the end of the Little Ice Age

(~AD 1900), MG has undergone almost continuous retreat (Knudsen et al. 2008). MG has reduced in area by 18 % (1986–2011), mean ice thickness by 22 % (1994–2012), volume by 30 % (1986–2011), and mean ice surface velocity by 30 %, which can be fully explained by the dynamic effect of ice thinning (Mernild et al. 2013a; Yde et al. 2014). Further, MG has undergone a surface elevation change where the vertical strain rate was able to compensate for ~50 % of the surface elevation lowering due to the surface mass-balance (SMB) conditions (Mernild et al. 2013a).

In this study, our aim is to address the knowledge gap in understanding the $B_a$ variability, with special focus on the variations between individual stake-observed $b_a$ mass-balance measurements. An improved understanding of long-term mass-balance variability is important to emphasize the link between glacier changes, meteorology and albedo feedbacks. We do this by analyzing a 19-year time series (1995/96–2013/14) of $b_a$ data from 34 individual MG long-term observation stakes. More specifically, we analyzed, mapped, and evaluated the patterns of both temporal and spatial MG $b_a$ variations using Empirical Orthogonal Functions (EOF). An EOF analysis allows us to describe simultaneously how spatial patterns of $b_a$ change over time among the 34 stakes. It is possible to combine the EOF output with a cross-correlation analysis of local and regional climate and geometric surface data to make hypotheses about the factors driving the spatiotemporal patterns of $b_a$ on MG. A detailed spatiotemporal mapping of $b_a$ variation is needed if we want to fully understand the factors influencing $B_a$ conditions and the impact on the hydrosphere in a “typical” Arctic landscape with a glacierized area, a downstream proglacial valley and outwash plain, and a delta and coastal zone (Hasholt and Jakobsen 2008).

To our knowledge this is the first time in Greenland an EOF analysis has been conducted on a local glacier scale to evaluate the spatiotemporal pattern in glacier $b_a$. MG mass-balance data up to 2010/11 have earlier been published in Mernild et al. (2013a), although only the $B_a$ was analyzed. EOF analysis has previously been applied in glacier studies by Mair et al. (2002) on Haut Glacier d'Arolla, Switzerland, who analyzed the spatiotemporal surface ice velocity field. Also, Walters and Meier (1989) and Mernild et al. (2015a) have analyzed the large-scale spatiotemporal variability of glacier $B_a$ conditions in western North America and along the Andes Cordillera to the sub-Antarctic islands, respectively. These analyses identified, for example, correlations between $B_a$ and large-scale atmospheric and oceanic indices.

## 2. Study area

Mittivakkat Gletscher formerly known as Midtluagkat Gletscher (26.2 km$^2$ in 2011); 65º41′ N, 37º48′ W) is located in the Ammassalik region, southeast Greenland (Figure 1). MG extends from 180 to 880 m above sea-level (a.s.l.) (Knudsen et al. 2008), and from 1986–2011 the mean surface slope changed from 5.4 degree to 5.9 degree. Approximately ~19 % of MG (4.9 km$^2$) had a slope between 6–10 degrees, ~20 % (5.2 km$^2$) between 11–15 degrees, ~ and ~18 % (4.8 km$^2$) between 16–20 degrees (for other slope intervals, see Table 1, Figure 2). With regards to aspect ~20 % (5.2 km$^2$) of the surface are facing towards the west, whereas ~14 % (3.8 km$^2$) are facing northwestwards and ~13 % (3.5 km$^2$) are facing southwestwards (for other slope intervals, see Table 1, Figure 2). Since 1995, the ELA has risen from ~350 m a.s.l. to ~>880 m a.s.l., with a mean ELA of ~750 m a.s.l. The ELA is the spatially averaged elevation of the equilibrium line, defined as the set of points on the glacier surface where the net mass-balance is zero. This ELA change has resulted in an average Accumulation Area Ratio (AAR) of 0.15 (Mernild et al. 2011). Hence, MG is significantly out of balance with the prevailing regional climate and will likely lose at least 70 % of its current area and 80 % of its volume even in the absence of further climate changes (Mernild et al. 2011).

Mean annual air temperature (MAAT) for the study period is -2.1°C (1993–2011) at Station Nunatak (Hanna et al. 2012; Mernild et al. 2014a), and mean annual corrected precipitation in the range of *c*. 1,400–1,800 mm water equivalent (w.e.) (1998–2006) (Mernild et al. 2008b) (precipitation was corrected after Allerup et al. 1998, 2000). For Station Tasiilaq a Danish Meteorological Institute (DMI) operated synoptic climate station located ~10 km southeast of MG (Station Tasiilaq is not shown on Figure 1), MAAT and mean annual precipitation sum changed (linear; both significant based on a linear regression *t*-test) ~0.8°C decade$^{-1}$ and ~-200 mm w.e. decade$^{-1}$, respectively (Hanna et al. 2012) . In this study, the term 'significant' is only used when the relationship is statistically significant at the 5 % level or better ($p \leq 0.05$).

## 3. Methods

### *3.1 Mass-balance program*

The stake network used to measure the MG net annual balance (Figure 1) is based on the direct glaciological method (Østrem and Brugman 1991); summer balance was calculated as the difference between the measured net annual balance and the measured winter balance. As the MG observations were started in the spring 1996 by measuring the winter accumulation along transects and stakes were later drilled into the snow and ice during the early summer, there are no direct observations of stake changes to determine net balance during the balance year 1995/96. This made it possible to determine the summer balance in late-august 1996. The 1995/96 net balance was determined as the winter balance subtracted the summer balance and not measured directly at stakes.

Since 1996/97, mass-balance measurements from individual stakes were obtained covering 16.3 $km^2$ of the main MG area, excluding the southeastern part of the glacier due to a high density crevassed area and the northern part of the glacier due to logistical reasons. This omission is not likely to bias the $B_a$ results as the surface of these areas follows the general hypsometric distribution of MG (Mernild et al. 2006). In total, 34 $b_a$ stakes were used for this study, where ~25 % have ≥15 annual observations during the period 1995/96–2013/14 and ~60 % have ≥10 (Figures 3 and 4). The locations of the stakes are shown in Figure 1 and cover the elevation range of MG. Direct $B_a$ observations are subject to uncertainties (where specifically year 2002 seems to be underestimated, see further below). The methodological uncertainty of $B_a$ estimates on a single glacier is, according to Zemp et al. (2013), in the range of ±340 mm w.e. This uncertainty is due to a combination of measurement and analytic errors and has been added to the data set.

*3.2 EOF analysis*

Empirical Orthogonal Function (EOF) analysis is a standard method in earth and marine sciences for exploring spatio-temporal variation in a variable. It is a principle components analysis applied to a data matrix organized by location (space) and time. The method has been applied to glaciological analyses several times (e.g., Walters and Meier 1989; Mernild et al. 2015a). In this study, the focus is on the spatiotemporal variability in $b_a$.

Our approach to estimating the EOFs implements Data Interpolating Empirical Orthogonal Functions (DINEOF; Beckers and Rixon 2003) because our data are 'gappy' with missing data in various years at various stakes. Our use of DINEOF via the R ‘sinkr’ package (https://github.com/marchtaylor/sinkr) fills gaps by iteratively decomposing the data field via singular value decomposition until a best solution is found as compared to a subset of reference values (Beckers and Rixon 2003; Taylor et al. 2013). We further extended the approach by interpolating and estimating the EOFs for our data 50 times and using the mean of these. This is because the interpolation process involves randomization and permutation.

As in any ordination technique, the major axes (e.g., EOF1 and EOF2) represent independent collections of information on the variable of interest, and in this case, variations in $b_a$ in space and time. The EOF analysis captures variations in $b_a$ simultaneously in time and space (Figure 4). The significance of the variations captured by each EOF can be evaluated several ways. These tools are designed to reveal how many major axes of variations there are in the data. We relied on bootstrap randomization approach to estimate the significance (see https://github.com/marchtaylor/sinkr).

The eigenvectors associated with such an analysis are linked to locations and thus reveal the influence of different geographic locations on the summarized mass-balance patterns and further allow analyses of meteorological covariates linked to the EOFs. All data were centered around zero and scaled to unit variance (Mernild et al. 2015a).

We first examined the eigenvectors (loadings) of the first EOF, which showed how this major axis of spatiotemporal variation in $b_a$ varies among stake locations. This provides a graphical visual summarization of the geographic patterns of temporal variation in $b_a$. The second assessment involved exploring how these correlations among sites and EOF varied regarding to site-specific characteristics such as elevation, slope, and aspect. The third assessment involved relating the temporal trends in EOFs to observed temporal trends in meteorological surface conditions. These trends include: i) observed MAAT (September through August; following the mass-balance year) and mean summer surface air temperature (June through August) from Station Nunatak; ii) observed MAAT, mean summer temperature, and winter precipitation sum (September through May) from Station Tasiilaq, and iii) the observed mean MG glacier-wide albedo.

The surface albedo is defined as the reflected fraction of incoming solar shortwave radiation (e.g., Dumont et al. 2012) and is a parameter that governs energy availability for snow and ice surface ablation, and subsequently variabilities in $b_a$ conditions. The mean MG glacier-wide surface albedo was estimated for a 16-day composite at the end of the mass-balance year period (27/28 July–12/13 August; 2000–2013), derived from the MODerate Imaging Spectroradiometer (MODIS MCD43A3) albedo product. For verification and technical details about the MODIS MCD43A3 MG albedo product, see Mernild et al. (2015b).

For estimation of MG surface slope and aspect a digital elevation model (DEM) was extracted from the Advanced Spaceborne Thermal Emission and Reflection Radiometer (ASTER) Global Digital Elevation Model Version 2 (GDEM v2) (based on the best observations between 2000 and 2010), with a vertical average precision of ~12 m over Greenland (Tachikawa et al. 2011). The vertical error was expected to be closer to the GDEM v2 standard ±8.7 m precision due to the gentle slope (<10 degrees) of the MG surface (Table 1) from where the measurements were taken (Tachikawa et al. 2011). The lateral error associated with GDEM v2 is a little more than half a pixel (17 m). The ASTER GDEM v2 is a product of the US Ministry of Economy, Trade, and Industry and NASA.

## 4. Results and discussion

*4.1 Variations in $B_a$ observations*

In Figure 5, the MG $B_a$ time series are shown. On average since 1995/96, annual $B_a$ was -1.00 ± 0.70 m water equivalent (w.e.) (where ± equals one standard deviation), indicating a cumulative mass-loss of 19 m w.e. (Figure 5). The MG $B_a$ loss has on average changed (linear) by -0.06 m w.e. $yr^{-1}$ (significant; $r^2 = 0.26$, where $r^2$ is the square of the linear correlation coefficient). Overall, in comparison to the other local glacier mass-balance programs in Greenland (even though different time periods were compared), the mean annual $B_a$ were negative for all observed glaciers: -0.55 ± 0.56 m w.e. Freya Gletscher (2007/08–2013/14) (Hynek et al. 2014), -0.40 ± 0.56 m w.e. Qaanaaq Gletscher (2012/13–2014/15) (Sugiyama et al. 2014), and -0.17 ± 0.34 m w.e. Qassinnguit Gletscher (2012/13–2014/15) (Abermann et al. 2014). Data were not available for A. P. Olsen Iskappe, as these data are too poorly constrained (pers. com., M. Citterio, September 2014). The available observed mean $B_a$ conditions indicate a 'snap-shot' in time for various periods, where a mean negative $B_a$ not only is a local phenomenon at MG, but present at other mass-balance observed glaciers in SE, NE, NW, and W Greenland.

In 2010/11, the $B_a$ at MG was at a record setting -2.45 m w.e. This was more than two standard deviations (-2$\sigma$; Figure 5) below mean. In both 2004/05 and 2009/10, $B_a$ was more than one standard deviation below mean (-1$\sigma$ ), and in 1995/96 and 2002/03 more than one standard deviation above mean (+1$\sigma$ ). These deviations were highly dominated both by relatively high mean summer temperature conditions and subsequently high ablation rates for 2004/05, 2009/10, and 2010/11 or enhanced winter precipitation conditions causing high accumulation rates for 1995/96 and 2002/03. Annual and seasonal variabilities in surface air temperature have in general an impact on the snow and firm temperature conditions (on the cold content), as temperature changes propagate into the snow and firn (e.g., Cuffey and Patterson 2010).

Therefore, high MAAT likely indicates a relatively lower end of winter season (May 31) snow cold content and subsequently contributing to an early start of the melt season.

When $B_a$ was either below (2004/05, 2009/10, and 2010/11) or above one standard deviation (1995/96 and 2002/03) between 66–100 % of the individual stake $b_a$ observations had values that were below or above one standard deviation, respectively. For the remaining 14 years, $B_a$ was within one standard deviation. Overall for the observation period, changes in glacier winter balance ($B_w$) and summer balance ($B_s$) explain 59 % and 90 % of the variability in $B_a$ (both significant; not shown), respectively. $B_w$ and $B_s$ were observed in 13 out of 19 years.

During the period 2004/05–2013/14, for example, seven of the highest recorded $B_a$ losses have occurred. During the past five years three of those losses were recorded in 2010/11, 2009/10 (-2.16 m w.e.), and 2011/12 (-1.63 m w.e.) (Figure 5). In terms of the mean surface summer air temperature, the period 2004/05–2013/14 had six and seven of the highest values observed at Station Nunatak and Station Tasiilaq, respectively (not shown). For Station Tasiilaq, the period 2004/05–2013/14 also included seven of the driest winters recorded (not shown), indicating that the climate in the MG region both got warmer and drier at the same time (Cappelen 2015; Mernild et al 2012a).

*4.2 Variations in* $b_a$ *observations*

The spatial distribution of mean MG observed $b_a$ 1996/97–2013/14 is illustrated on Figure 6a. Observed mean $b_a$ values were lowest ~-3.0 m w.e. at the lowest MG elevations close at the margin (180 m a.s.l.) and ~-0.5 m w.e. at the highest elevations (~650 m a.s.l.), indicating net ablation everywhere on the glacier. The mean annual $b_a$ value of -1.0 m w.e. was observed at ~500 m a.s.l., whereas mean $b_a$ lower than -1$\sigma$ (-1.7 m w.e.) and -2$\sigma$ (-2.4 m w.e.) were observed at elevations lower than ~400 m a.s.l. and ~300 m a.s.l., respectively (Figure 6a). The spatial and longitudinal distributions of observed $b_a$ variability (1$\sigma$) are illustrated in Figures 6b and 6e, respectively, indicating that the temporal variability in $b_a$ increased in value with increasing elevation until 300–400 m a.s.l. Above this elevation the variability in $b_a$ decreased slightly. In the frontal area below 200 m a.s.l., the mean $b_a$ standard deviation was 0.48 m w.e. and above 600 m a.s.l. it was 0.77 m w.e. The highest temporal variability of 0.85–0.88 m w.e. was present at elevations between 300–600 m a.s.l. (Figure 6e). This peak in $b_a$ variability at elevations between 300–600 m a.s.l. along the central part of the glacier was likely identical to the average ascent of the ELA over the observation period (Mernild et al. 2015b), probably because the variability in $b_a$ was influenced by the combined effects of changes in winter and summer meteorological conditions. This elevation range (300–600 m a.s.l.) was also the area, where the greatest change (-0.25) in the observed end of mass-balance year albedo occurred, identifying this zone as an important surface cover and albedo transitional zone – an ELA zone (Mernild et al. 2015b). The lowest variations in $b_a$ together with the lowest changes in surface albedo both occurred where MG was either snow covered at the end of the mass-balance year (in the high-elevation accumulation zone) or constituted of exposed glacier ice (in the low-elevation ablation zone). Hence, in case the variability in $b_a$ followed the -1$\sigma$ or +1$\sigma$ variability for a specific year, $b_a$ values in the frontal area would be as low as ~-3.5 m w.e. and at approximately 525 m a.s.l. ~-1.8 m w.e. for -1$\sigma$ (Figure 6c), and ~-2.6 m w.e. and ~0 m w.e. (identical with the location of the ELA) for +1$\sigma$ (Figure 6d), respectively. In other words, $b_a$ followed the upper and lower boundaries of the longitudinal profile as illustrated in Figure 6e.

*4.3 $b_a$ observations and EOF variance analysis*

In Figure 3, the annual observed $b_a$ time series are shown for all 34 individual stakes on MG. Overall, the variability in the $b_a$ time series occurred both for each individual time series and between the annual stake values. For some years such as 2002/03 ($\sigma = 0.45$ m w.e.), 2005/06 ($\sigma = 0.60$), and 2010/11 ($\sigma = 0.37$) marked with blue colored squares in Figure 3, the $b_a$ spatial variability was relatively low compared to other years 2000/01 ($\sigma = 1.04$), 2001/02 ($\sigma = 1.10$), and 2012/13 ($\sigma = 1.09$) marked with red colored circles. This indicates that for the first three highlighted years relatively homogeneous $b_a$ conditions and a low $b_a$ gradient existed, and opposite for the last three highlighted years. The years with relatively negative $B_a$ (Figure 5) were the years with relatively low spatial variability in $b_a$ (i.e., relatively homogeneous $b_a$ conditions, Figure 3), and opposite for years with less negative or positive $B_a$ ($r^2 = 0.43$, significant).

In Figure 7, we report on two major axes (modes) estimated from our EOF analysis of spatiotemporal variation: EOF1 and EOF2 representing 80 % (significant) and 6 % (insignificant) of the explained variance, respectively. The temporal and spatial variability in EOF1 and EOF2 are illustrated in Figures 7 and 8, respectively. Regarding EOF1, we show a five-year running mean smoothing line that increased over the time-period, being negative until 2003 and positive thereafter (Figure 7). For EOF2 the five-year running mean smoothing line oscillated with an approximately six-year frequency. EOF2 was negative during the periods 1995–1999, 2003–2006, and 2009–2012 and positive during the periods 1999–2003, 2006–2009, and after 2012. Hence, the EOF2 five year running mean smoothing line was more complex than the EOF1 pattern.

Both the temporal EOF1 and EOF2 patterns were associated with individual eigenvectors for each individual stake (Figure 8). For EOF1, the bar-plot in Figure 8 illustrates negative values for *all* stakes, indicating that EOF1 was capturing increasing mass loss at all stakes and therefore decreasing annual $B_a$ loss. These negative correlations emphasize that variations in mass-loss were uniformly distributed in space and time at all stakes (Figures 8a and 9a).

We found that EOF1 showed a significant correlation with Station Nunatak mean summer air temperature and glacier-wide albedo (Figure 10 and Table 2). However, we also noted that values at year 2002 were a statistical outlier (due to an underestimation of measured $b_a$). As an example, if we ignore the year 2002 values EOF1 was correlated with MAAT and mean summer air temperature from both Station Nunatak and Station Tasiilaq and observed mean glacier-wide albedo, but not winter precipitation sum from Station Tasiilaq (Figure 11 and Table 2). We suggest that EOF1 strongly reflected variability in air temperature conditions and albedo, rather than variability in precipitation conditions and topographic conditions. None of the correlations to precipitation at both Station Nunatak and Station Tasiilaq were significant (Table 2). We suggest that this is because precipitation in Greenland varies according to the topography and the patterns of weather systems and even within short distances precipitation is likely explained by prevailing wind circulation e.g., katabatic winds draining downslope from the ice-sheet interior, distance from the oceanic moisture source and the orographic effect of near-coastal mountains. The latter is especially important in Southeast Greenland (e.g., Hansen et al. 2008) and in the area of MG, where the mean corrected annual precipitation varies from ~1,250 mm w.e. (1999–2006) (uncorrected ~900 mm w.e.) at Station Tasiilaq to ~1,850 mm w.e. at Station Nunatak (1999–2006) (Mernild et al. 2008b, 2015c).

Station Tasiilaq is located around 10 km southeast of MG and highly influenced by maritime climate conditions, having a mean monthly air temperature range of 10–15ºC (Cappelen et al. 2015). In comparison, Station Nunatak was influenced by coastal climate conditions, having a mean monthly air temperature range of 15–25ºC (Mernild et al. 2008b). At MG the $B_a$ variability is significantly correlated with variabilities in both maritime and coastal climate conditions (for definitions of maritime and coastal climate conditions, see Przybylak 2003). It therefore seems very likely that similar variabilities in $B_a$ may occur for other glaciers located within maritime and coastal climate conditions in Southeast Greenland. Due to the significant correlation between MG $B_a$ and observed air temperature both at Station Nunatak and Station Tasiilaq – two stations located in different climate conditions –, we propose that variability in $B_a$ is not only a local phenomenon. Mernild et al. (2011) found that MAAT time series from Southeast Greenland's coastal DMI stations were significantly correlated with MAAT time series from Station Tasiilaq. These data further suggest that $B_a$ variability at MG, which has been driven largely by surface air temperature variabilities, is representative for mass-balance variations on a regional scale, which includes many hundreds of local glaciers. In support of this statement, the trends in glacier terminus recession at MG and mass-balance conditions are on average similar to glacier terminus recessions for land-terminating glaciers in the Ammassalik region (Mernild et al. 2012b) and overall for land-terminating glaciers in Southeast Greenland (Bjørk et al. 2012), and to simulated mass-balance conditions in the Ammassalik region (Mernild et al. 2014b), respectively.

In contrast to the EOF1 dataset, the EOF2 pattern was complex and showed a more spatial variable pattern with in total 11 (shown with light gray color) out of 34 stakes (~33 % of the stakes) being in phase with EOF2 and 23 stakes (~67 % of the stakes) being out of phase with EOF2 (dark gray; Figure 8b). While our bootstrap analysis indicates that the 6 % of variation captured by EOF2 is not significant given the current set of data, we explore it because the EOF2 pattern was complex and showed a more spatial variable pattern than the EOF1 dataset; we note these thus represent hypotheses about more localized patterns in $b_a$.

Surface elevation, slope, and aspect explained none of the $b_a$ site-specific correlations with EOF1, but they explained variation in the spatial component of EOF2 (Figures 9a–9c). We suggest that the 11 stakes being in phase with EOF2 may have different mean geometrical surface terrain features such as different mean surface slope and aspect than the other 23 stakes in the mass-balance network. In general, we found that the 11 stakes being in phase with EOF2 likely had lower mean surface slope than the other 23 stakes being out of phase with EOF2 (see also Figure 9b). For these 11 stakes, the mean surface slope was 8.5 degrees, whereas the mean slope at the other 23 stakes was 11.0 degrees (significant not equal). Further, our analysis indicates that the stakes being in phase with EOF2 mainly had south facing aspects; whereas stakes being out of phase with EOF2 mainly had west and north facing aspects (see also Figure 9c). Even though the EOF2 pattern probably can be explained by the variability in surface conditions – by the mean surface slope and/or aspect, the more general EOF1 pattern seemed to be dominated by other controls than surface characteristics such as variations in meteorological conditions.

Further, EOF2 indicated a general eigenvector correlation pattern related to elevations on MG, where low-elevated stakes (~<400 m a.s.l.) showed relatively negative (out of phase) eigenvector correlation values and higher elevated stakes relatively positive (in phase) eigenvector correlation values (Figure 9a). Such relatively negative and positive eigenvector correlation values were present where MG either constituted of exposed glacier ice in the low-elevated ablation zone or snow cover in the high-elevated accumulation zone during $b_a$ observations. Also, these patterns were likely related to changes in both MG snow cover duration and the occurrence of frequent air temperature inversion on the lower part of MG (~<300 m a.s.l.): Inversion and sea breezes associated with the adjacent relatively low temperature and frequently ice-chocked fjords and oceans (Mernild and Liston 2010). Observations indicate that air temperature inversion is to be present 84 % of the time, and essential for accumulation and surface ice melt conditions (Mernild and Liston 2010). Therefore, in general these EOF2 stake eigenvector correlations likely indicated a change from eigenvectors being out of phase to eigenvector being in phase with increasing elevation, even though minor fluctuations in eigenvector correlations occurred due to variations in both surface slope and aspect (even within a distance less than a few hundred of meters). The EOF2 correlation values emphasize that variations in mass-loss were heterogeneously distributed (insignificant) in space and time at the MG stakes.

An understanding of such MG EOF correlations – its variability to changes in climate and surface conditions – is of interest for different purposes because local glaciers in Greenland are less well-studied than the Greenland Ice Sheet, but also for mass-balance upscaling proposes to regions from where no glacier mass-balance observations are available.

## 5. Conclusions

Our findings show that in 14 out of 19 years, $B_a$ was within one standard deviation with a mean annual loss of -1.00 ± 0.70 m w.e., a change of -0.06 m w.e. $yr^{-1}$ during a period of climate warming and drying, following the variability in AMO (Mernild et al. 2012a). Relatively negative MG $B_a$ equal low spatial variability in $b_a$. A change in $B_a$ indicates that the greatest variability in $b_a$ occurred for stakes located between 300–600 m a.s.l. and is likely related to the ascent of the ELA.

The EOF analysis is a robust way of obtaining spatiotemporal information on glacier mass-balance patterns. The use of a statistical EOF variance analysis suggests that observed $b_a$ on MG in time and space can be summarized by a single major axis of variation EOF1 representing 80 % (significant) of the explained variance. Further, EOF1 emphasizes variations in $b_a$ related to variations in albedo and surface air temperature observations from nearby maritime and coastal stations. However, we also explore the second major axis, which explained 6 %, because it suggests possible localized geographic effects on $b_a$ linked to surface conditions associated with slope and aspect. Our EOF calculations are crucial for our understanding of spatiotemporal mass-balance variabilities and for mass-balance upscaling possibilities in Greenland because variabilities in $b_a$ are influenced strongly by variabilities in summer air temperature and MAAT and mean glacier-wide observed albedo, and insignificant against surface characteristics such as slope and aspect. Additionally, it is crucial for our understanding – in case of upscaling to regions with no observations – because we have few mass-balance observations from local glaciers in Greenland.

**Acknowledgements**

We thank Japan Society for Promote Science (JSPS) for support, under grant agreement No. S17096. Also, we thank InterAct for support, under the project: ALBICE, where the research leading to these results has received funding from the European Union's Horizon 2020 project INTERACT, under grant agreement No. 730938. We thank the all the people who have participated in the Mittivakkat Gletscher mass-balance fieldwork over the years. Finally, we thank the Danish Meteorological Institute for providing World Meteorological Organization synoptic meteorological data from Tasiilaq, and University of Copenhagen for providing meteorological data from and around the Mittivakkat Gletscher.

## References


Abermann, J., van As, D., Petersen, D., and Nauta, M. 2014. A new glacier monitoring site in West Greenland. *Abstract AGU Fall meeting*, December 2014.

Allerup, P., Madsen, H., and Vejen, F. 1998. Estimating true precipitation in arctic areas. In *Proceedings of the Nordic Hydrological Conference*. Helsinki: Nordic Hydrological Programme Report, 44, 1–9.

Allerup, P., Madsen, H., and Vejen, F. 2000. Correction of precipitation based on off-site weather information. *Atmos. Res.* 53, 231–250.

Allison, I., Colgan, W., King, M., and Paul, F. 2015. Ice Sheets, Glaciers, and Sea Level (Chapter 20). In Snow and Ice-Related Hazards, Risks, and Disasters, (ed.) Haeberli, W., Whiteman, C., and Shroder, J. F., Elsevier, Amsterdam, 713–747.

AMAP, 2017. Snow, Water, Ice and Permafrost. Summary for Policy-makers. Arctic Monitoring and Assessment Programme (AMAP), Oslo, Norway. 20 pp

Beckers, J.-M. and Rixen, M. 2003. EOF Calculations and Data Filling from Incomplete Oceanographic Datasets. *Journal of Atmospheric and Oceanic Technology,* 20(12), 1839–1856.

Bjørk, A. A., Kjær, K. H., Korsgaard, N. J., Khan, S. A., Kjeldsen, K. K., Andresen, C. S., Box, J. E., Larsen, N. K., and Funder, S. 2012. An areal view of 80 years of climate-related glacier fluctuations in Southeast Greenland. *Nature Geoscience*, 5, 427–432.

Cappelen, J. 2015. Greenland - DMI Historical Climate Data Collection 1784-2014. Technical Report DMI, 15-04, pp. 97. www.dmi.dk/fileadmin/user_upload/Rapporter/TR/2015/tr15-04.pdf

Chylek, P., Folland, C., Lesins, G.,Wang, M. and Dubey, M. 2009. Arctic air temperature change amplification and the Atlantic multidecadal oscillation. *Geophysical Research Letter*, 36, L14801.

Cogley, J. G. 2012. The future of the world's glaciers. The Future of the World's Climate, 2nd ed., A. Henderson-Sellers and K. McGuffie, Eds., Elsevier, 205–218, doi:10.1016/B978-0-12-386917-3.00008-7.

Cuffey, K. M. and Patterson, W. S. B. 2010 The Physics of Glaciers. Fourth Edition. Oxford, pp. 693.

Dumont, M., Gardelle, J., Sirguey, P., Guillot, A., Six, D., Rabatel, A., and Arnaud, Y. 2012. Linking glacier annual mass balance and glacier albedo retrieved from MODIS data. *Cryosphere,* 6, 1527–1539, doi:10.5194/tc-6-1527-2012.

Fristrup, B. 1970. New Geographical Station in Greenland. *Geografisk Tidsskrift-Danish Journal of Geography*, 69, 199–203.

Gardner, A. S., and Coauthors 2013. A reconciled estimate of glacier contributions to sea level rise: 2003 to 2009. *Science*, 340, 852–857, doi:10.1126/science.1234532.

Hanna, E., Mernild, S. H., Cappelen, J., and Steffen, K. 2012. Recent warming in Greenland in a long-term instrumental (1881–2012) climatic context. Part 1: Evaluation of surface air temperature records. *Environmental Research Letters*, 7, 045404, doi:10.1088/1748-9326/7/4/045404.

Hansen, B. U., Sigsgaard, C., Rasmussen, L., Cappelen, J., Hinkler, J., Mernild, S. H., Petersen, D., Tamstorf, M., Rasch, M. and Hasholt, B. 2008. Present Day Climate at Zackenberg. *Advances in Ecological Research*, 40, 115–153.

Hasholt, B., and Jakobsen, B. H. 2008. 75 years of research at the Sermilik Station: 1933–2008. *Geografisk Tidsskrift-Danish Journal of Geography*, 108, 1–4.

Hynek, B., Weyss, G. Binder, D., and Schöner, W. 2014. Mass Balance of Freya Glacier, 2007/2008-2012/2013. *Pangea*, doi:10.1594/PANGAEA.831035.

Kaplan, A., Cane, M., Kushnir, Y., Clement, A., Blumenthal, M., and Rajagopalan, B. 1998. Analyses of global sea surface temperature 1856–1991. *Journal of Geophysical Research*, 103, 18,567–18,589.

Kargel, J. S., Ahlstrøm, A. P., Alley, R. B., Bamber, J. L., Benham, T. J., Box, J. E., Chen, C., Christoffersen, P., Citterio, M., Cogley, J. G., Jiskoot, H., Leonard, G. J., Morin, P., Scambos, T., Sheldon, T., and Willis, I. 2012. Brief communication Greenland's shrinking ice cover: "fast times" but not that fast. *The Cryosphere*, 6, 533–537.

Knudsen, N. T., Nønberg, P., Yde, J. C., Hasholt, B., and Heinemeier, J. 2008. Recent marginal changes of the Mittivakkat Glacier, Southeast Greenland and the discovery of remains of reindeer (*Rangifer tarandus*), polar bear (*Ursus maritimus*) and peaty material. *Geografisk Tidsskrift-Danish Journal of Geography*, 108(1), 137–142

Leclercq, P. W., Oerlemans, J., and Cogley, J. G. 2011. Estimating the glacier contribution to sea-level rise for the period 1800–2005. *Surv. Geophys.*, 32, 519–535, doi:10.1007/s10712-011-9121-7.

Larsen, S. H., Citterio, M., Hock, R., and Ahlstrom, A. P. 2012. Mass and surface energy balance of A.P. Olsen ice cap, NE Greenland, from observations and modeling (1995–2011). *Abstract AGU Fall meeting,* C23B-0660.

.

Machguth, H., Thomsen, H. H., Weidick, A., Abermann, J., Ahlstroem, A. P., Andresen, M. L., Andersen, S. B., As, D. van, Boeggild, C. E., Box, J. E., Braithwaite, R. J., Citterio, M., Clement, P., Colgan, W., Fausto, R. S., Gleie, K. Hasholt, B., Hynek, B., Knudsen, N. T., Mernild, S. H., Oerter, H., Olesen, O. B., Steffen, K., Stober, M., Sugiyama, S., and van de Wal, R. S. W. 2016. A comprehensive database of Greenland surface mass balance observations from the ice sheet ablation area and the local glaciers. Accepted *Journal of Glaciology.*

Mair, D., Nienow, P., Sharp, M., Wohlleben, T., and Wills, I. 2002. Influence of subglacial drainage system evolution on glacier surface motion: Haut Glacier d'Arolla, Switzerland. *Journal of Geophysical Research – Solid Earth*, 107(B8), 1-13, 10.1029/2001JB000514.

Marzeion, B., Jarosch, A. H., and Hofer, M. 2012. Past and future sea-level change from the surface mass balance of glaciers. *Cryosphere*, 6, 1295–1322, doi:10.5194/tc-6-1295-2012.

Mernild, S. H., Hanna, E., McConnell, J. R., Sigl, M., Beckerman, A. P., Yde, J. C., Cappelen, J., and Steffen, K. 2015c. Greenland precipitation trends in a long-term instrumental climate context (1890–2012): Evaluation of coastal and ice core records. *International Journal of Climatology*, 35, 303–320, doi:10.1002/joc.3986.

Mernild, S.H., Hanna, E., Yde, J.C., Cappelen, J., and Malmros, J.K. 2014a. Coastal Greenland air temperature extremes and trends 1890–2010: annual and monthly analysis. *International Journal of Climatology*, 34, 1472–1487, doi:10.1002/joc.3777.

Mernild, S. H., Hansen, B. U., Jakobsen, B. H., and Hasholt, B. 2008b. Climatic conditions at the Mittivakkat Glacier catchment (1994–2006), Ammassalik Island, SE Greenland, and in a 109 years term perspective (1898–2006). *Geografisk Tidsskrift-Danish Journal of Geography,* 108(1): 51–72.

Mernild, S. H. and G. E. Liston 2010. The influence of air temperature inversion on snow melt and glacier surface mass-balance simulations, SW Ammassalik Island, SE Greenland. *Journal of Applied Meteorology and Climate*, 49(1), 47–67.

Mernild, S. H., Liston, G. E., Hasholt, B., and Knudsen, N. T. 2006. Snow distribution and melt modeling for Mittivakkat Glacier, Ammassalik Island, SE Greenland. *Journal of Hydrometeorology*, 7, 808–824.

Mernild, S. H., Liston, G. E., and Hiemstra, C. A. 2014b. Northern Hemisphere glaciers and ice caps surface mass balance and contribution to sea-level rise. *Journal of Climate*, 27(15), 6051–6073, doi.org/10.1175/JCLI-D-13-00669.1.

Mernild, S. H., Knudsen, N. T., Hoffman, M. J., Yde, J. C., Lipscomb, W. L., Hanna, E., Malmros, J. K., and Fausto, R. S. 2013a. Volume and velocity changes at Mittivakkat Gletscher, Southeast Greenland, 1994–2012. *Journal of Glaciology,* 59(216), 660–670, doi:10.3189/2013JoG13J017.

Mernild, S. H., Knudsen, N. T., Lipscomb, W. H., Yde, J. C., Malmros, J. K., Jakobsen, B. H., and Hasholt, B. 2011. Increasing mass loss from Greenland's Mittivakkat Gletscher. *The Cryosphere*, 5, 341–348: doi:10.5194/tc-5-341-2011.

Mernild, S. H., Lipscomb, W. H., Bahr, D. B., Radić, V., and Zemp, M. 2013b. Global glacier retreat: A revised assessment of committed mass losses and sampling uncertainties. *The Cryosphere*, 7, 1565–1577, doi:10.5194/tc-7-1565-2013.

Mernild, S. H., Beckerman, A. P., Yde, J. C., Hanna, E., Malmros, J. K., Wilson, R., and Zemp, M. 2015a. Mass loss and imbalance of glaciers along the Andes to the sub-Antarctic islands. *Global and Planeratary Change*, 133, 109–119: doi:10.1016/j.gloplacha.2015.08.009.

Mernild, S. H., Malmros, J. K., Yde, J. C., and Knudsen, N. T. 2012b. Multi-decadal marine and land-terminating glacier retreat in Ammassalik region, Southeast Greenland. *The Cryosphere*, 6, 625–639, doi:10.5194/tc-6-625-2012.

Mernild, S. H., Malmros, J. K., Yde, J. C., Knudsen, N. T., Wilson, R., Hanna, E., Fausto, R. S., van As, D. 2015b. Albedo decline on Greenlands Mittivakkat Gletscher. *International Journal of Climatology*, 35, 2294–2307, doi: 10.1002/joc.4128.

Mernild, S. H., Seidenkrantz, M.-S., Chylek, P., Liston, G. E., and Hasholt, B. 2012a. Climate-driven fluctuations in freshwater to Sermilik Fjord, East Greenland, during the last 4000 years. *The Holocene,* 22(2), 155–164, doi:10.1177/0959683611431215.

Pfeffer, T. W., Arendt, A. A., Bliss, A., Bolch, T., Cogley, J. G., Gardner, A. S., Hagen, J.-O., Hock, R., Kaser, G., Kienholtx, C., Miles, E. S., Moholdt, G., Molg, N., Paul, F., Radić**,** V., Rastner, P., Raup, B. H., Ricj, J., Sharp, M. J., The Randolph Consortium, 2014. The Randolph Glacier Inventory: a globally complete inventory of glaciers. *Journal of Glaciology*, 60(221), 537–552.

Przybylak, R. 2003. *The climate of the Arctic*. Kluwer Academic Publishers, Atmospheric and Oceanographic Sciences Library 26, 270 pp.

Radić, V., Bliss, A., Beedlow, A. C., Hock, R., Miles, E., and Cogley, J. G. 2014. Regional and global projection of twenty-first century glacier mass changes in response to climate scenarios from global climate models. *Climate Dynamics*, 42, 37–58.

Rastner, P., Bolch, T., Mölg, N., Machguth, H., Le Bris, R., and Paul. F. 2012. The first complete inventory of the local glaciers and ice caps on Greenland. *The Cryosphere*, 6, 1483–1495, doi:10.5194/tc-6-1483-2012.

Sugiyama, S. Sakakibara, D., Matsuno, S., Yamaguchui, S., Matoba, S., and Aoki, T. 2014. Initial field observations on Qaanaaq ice cap, northwestern Greenland. *Annals of Glaciology*, 55(66), 25–33.

Tachikawa, T. and 12 others (ASTER GDEM Validation Team) 2011. *ASTER Global Digital Elevation Model Version 2 – summary of validation results, NASA Land Processes.* NASA Distributed Active Archive Center, Joint Japan–US ASTER Science Team, http://www.jspacesystems.or.jp/ersdac/GDEM/ver2Validation/Summary_GDEM2_validation_report_final.pdf

Taylor, M. H., Losch, M., Wenzel, M., and Schroeter, J. 2013. On the sensitivity of field reconstruction and prediction using Empirical Orthogonal Functions derived from gappy data. *Journal of Climate*, 26, 9194–9205.

Walters, R. A. and Meier, M. F. 1989. Variability of glacier mass balances in western North America, in aspects of climate variability in the Pacific and the western Americas (ed. D. H. Peterson), American Geophysical Union, Washington, D. C., doi: 10.1029/GM055p0365.

Weidick, A., and Morris, E., 1998. Local glaciers surrounding the continental ice sheets. In Haeberli, W., Hoelzle, M., and Suter, S. (eds.), *Into the second century of world glacier monitoring – prospects and strategies*. Paris: UNESCO. UNESCO Studies and Reports in Hydrology, 56, 167–176.

Yde, J. C., Gillespie, M. K., Løland, R., Ruud, H., Mernild, S. H., de Villiers, S., Knudsen, N. T. and Malmros, J. K. 2014. Volume measurements of Mittivakkat Gletscher, southeast Greenland. *Journal of Glaciology*, 60(224), 1199-1207, doi: 10.3189/2014JoG14J047.

Zemp, M., Frey, H., Gartner-Roer, I., Nussbaumer, S. U., Hoelzle, M., Paul, F., Haeberli, W., Denzinger, F., Ahlstrom, A. P., Anderson, B., Bajracharya, S., Baroni, C., Braun, L. N., Caceres, B. E., Casassa, G., Cobos, G., Davila, L. R., Granados, H. D., Demuth, M. N., Espizua, L., Fischer, A., Fujita, K., Gadek, B., Ghazanfar, A., Hagen, J. O., Holmlund, P., Karimi, N., Li, Z., Pelto, M., Pitte, P., Popovnin, V. V., Portocarrero, C. A., Prinz, R., Sangewar, C. V., Severskiy, I., Sigurdsson, O., Soruco, A., Usubaliev, R., and Vincent, C. 2015: Historically unprecedented global glacier decline in the early 21st century. *Journal of Glaciology*, 61(228), 745–762, doi: 10.3189/2015JoG15J017.

Zemp, M., Thibert, E., Huss, M., Stumm, D., Rolstad Denby, C., Nuth, C., Nussbaumer, S. U., Moholdt, G., Mercer, A., Mayer, C., Joerg, P. C., Jansson, P., Hynek, B., Fischer, A., Escher-Vetter, H., Elvehøy, H. and Andreassen, L. M. 2013. Uncertainties and re-analysis of glacier mass balance measurements. *The Cryosphere*, 7, 1227–1245.

Østrem, G. and Brugman, M. 1991: Glacier mass-balance measurements: a manual for field and office work. NHRI Science Report 4. Environment Canada. National Hydrology Research Institute, Saskatoon, Sask.

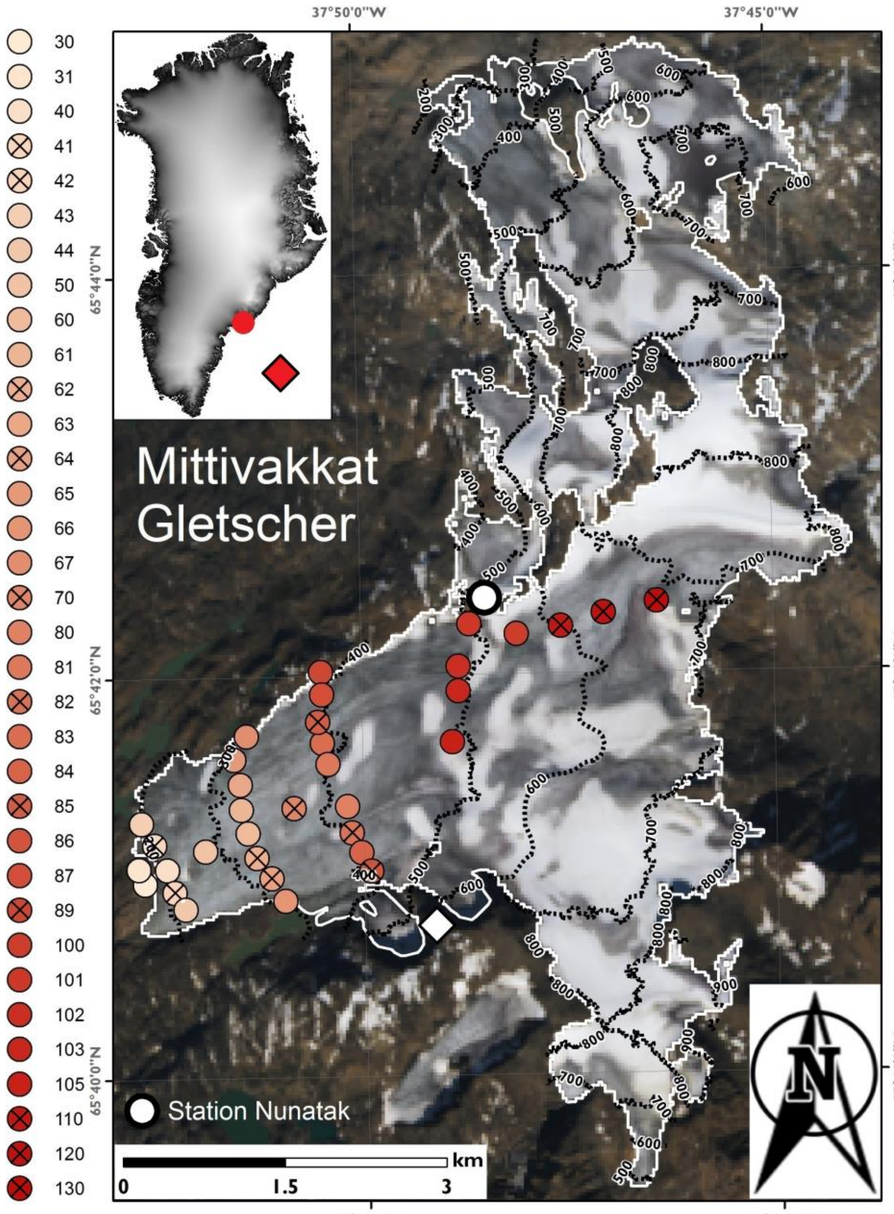


**Figure 1:** Mittivakkat Gletscher (26.2 km$^2$ (2011); 65°41′N, 37°48′W) topographic map (100-m contour interval). The colored circles illustrate the 34 stake locations for the ongoing glacier mass-balance observation program, 1995/96–2013/14. The stake colors on the glacier surface correspond to the stake numbers illustrated to the left, where the low numbers correspond to the stakes at the low-elevation part of the glacier. Stakes in anti-phase for the EOF2 analysis are shown with a cross. Station Nunatak (515 m a.s.l.) is illustrated with a white circle. Station Tasiilaq is not included as it is located ~10 km southeast of the glacier. The white diamond indicates the location where the photo in Figure 2c was taken. Source: Landsat 8, OLI (Operational Land Imager), 7 August 2014.

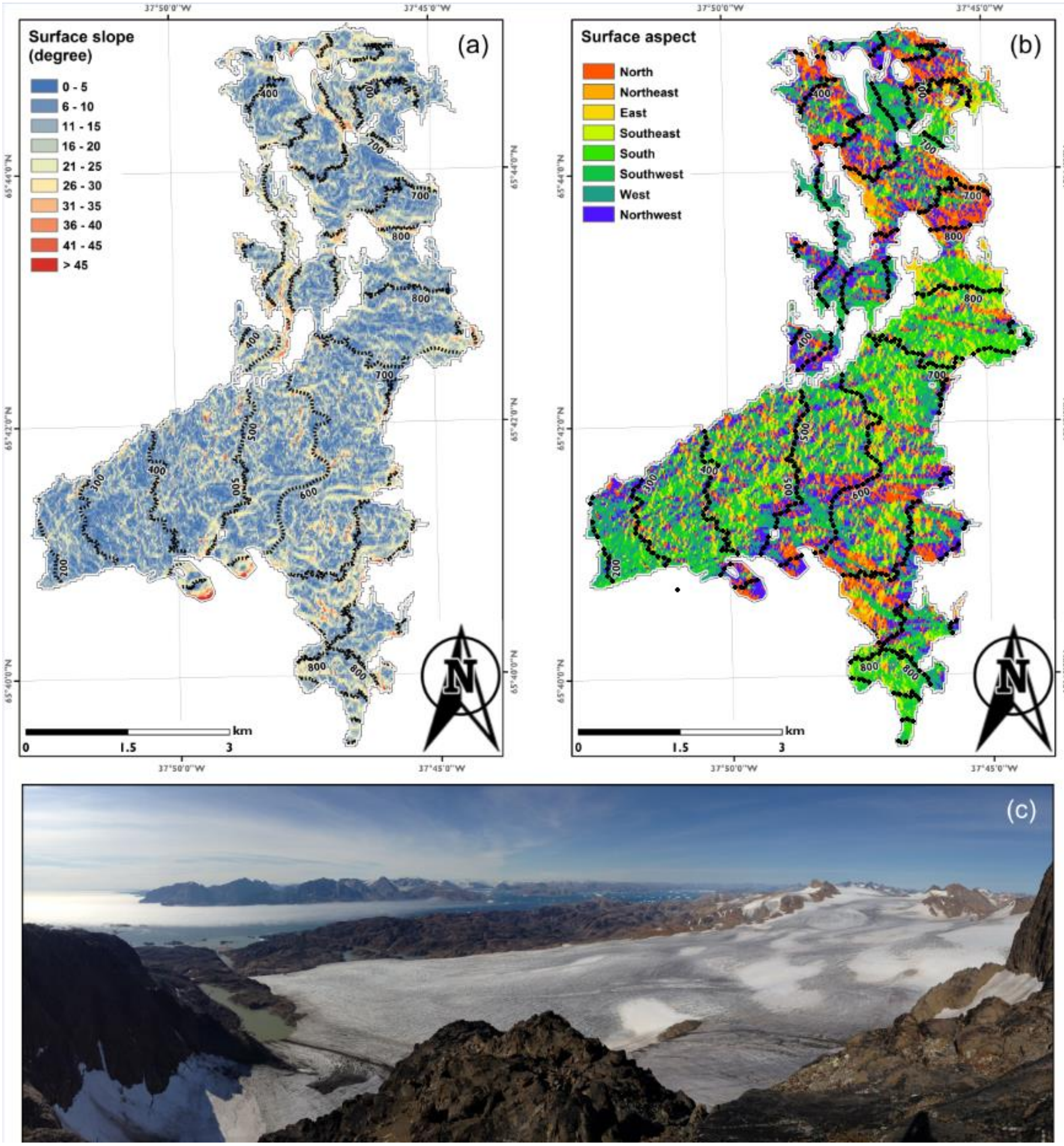


**Figure 2:** Mittivakkat Gletscher: (a) surface slope; (b) surface aspect; and (c) photo of the southwestern part of the glacier (the photo was taken looking north northwest, and in the background is Sermilik Fjord and the Greenland Ice Sheet, photo M. Lidström, August 2014). Area values for each slope and aspect interval are shown in Table 1. Surface slope and aspect is constructed based on the Advanced Spaceborne Thermal Emission and Reflection Radiometer (ASTER) Global Digital Elevation Model Version 2 (GDEM v2). The glacier margin outline is from 7 August 2014.

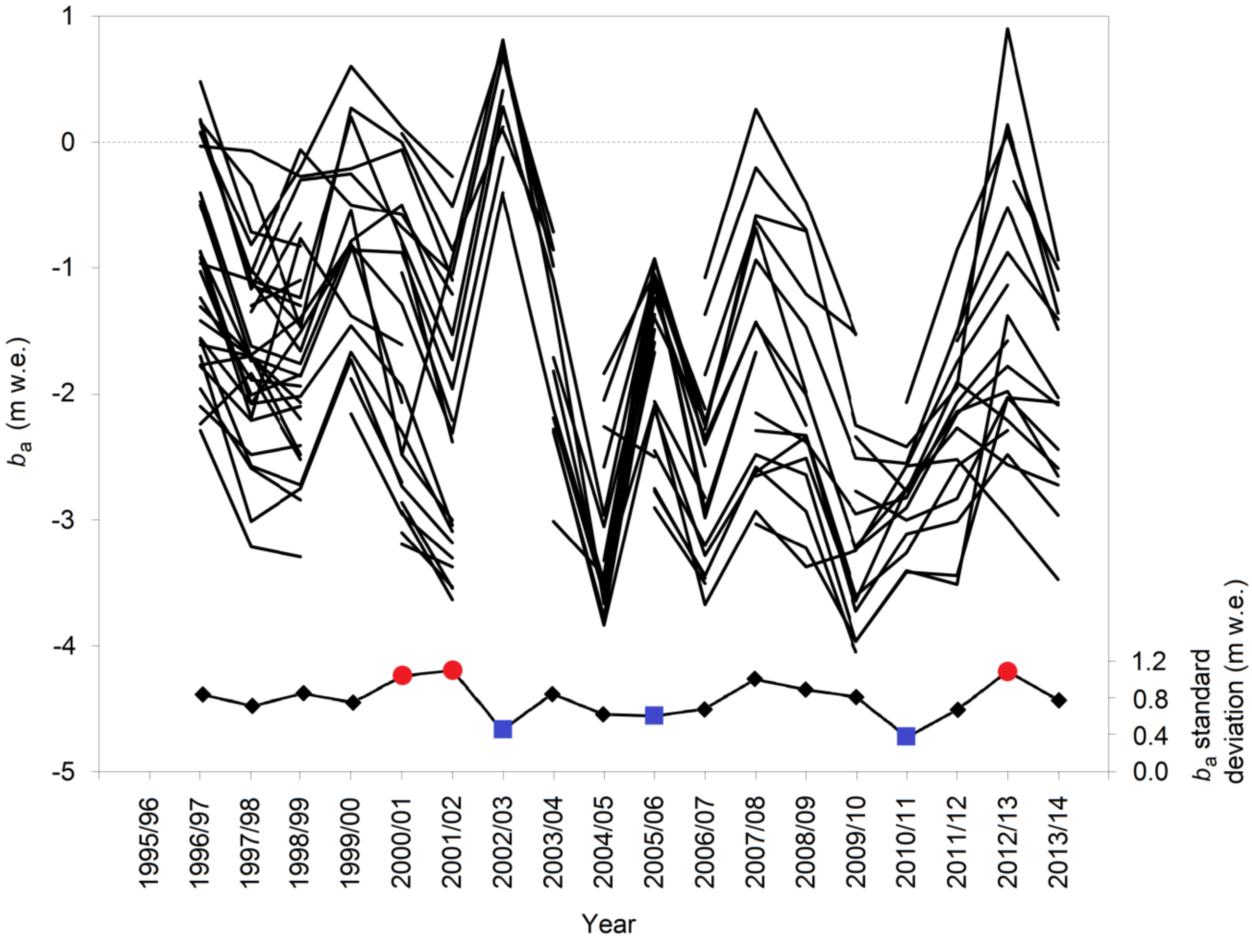


**Figure 3:** Time series of individual observed $b_a$ time series from Mittivakkat Gletscher for the period 1996/97–2013/14, including calculated annual variability of $b_a$ (at the bottom). The three maximum and minimum annual variabilities are marked with red circles and blue squares, respectively.

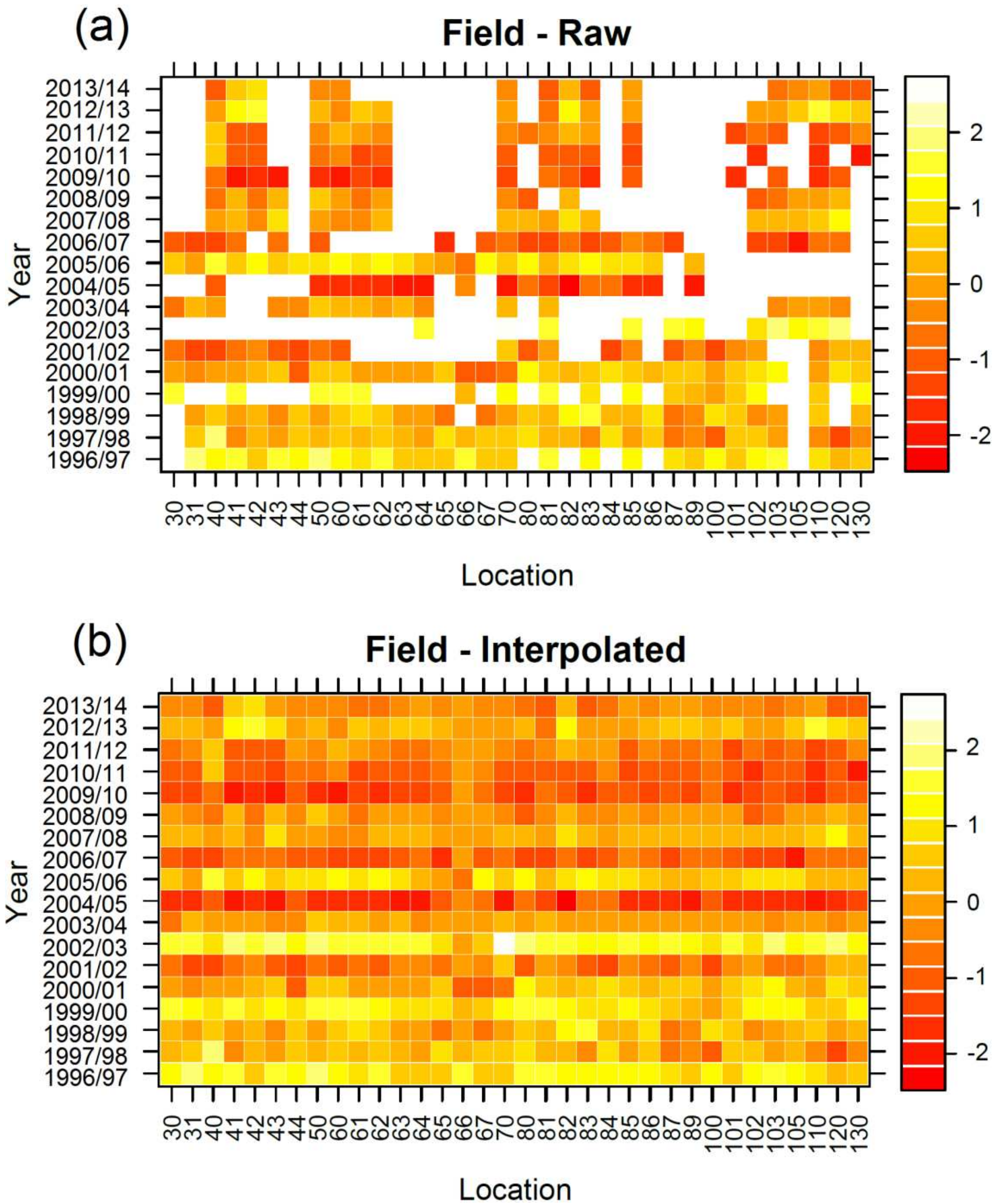


**Figure 4:** Space-time field (1996/97–2013/14) for Mittivakkat Gletscher, where the stake locations from left to right go from lowest stake numbers to highest stake number: (a) raw data field (the white squares equal no data): and (b) reconstructed data field. The reconstructed field is the mean of replicate reconstructions using the DINEOF method.

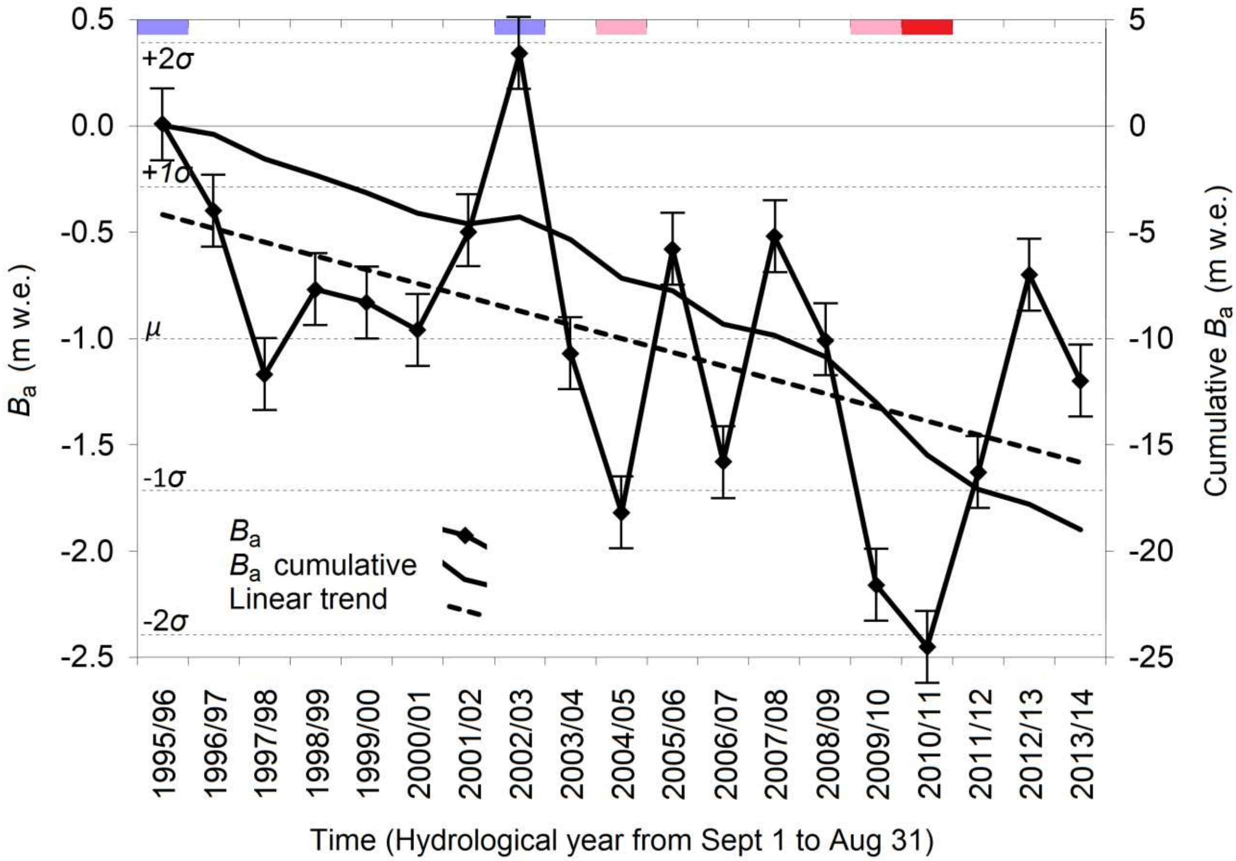


**Figure 5:** Observed $B_a$, cumulative $B_a$, and linear trend for $B_a$ for Mittivakkat Gletscher (1995/96–2013/14). The colors light blue and pink indicated $B_a$ values one standard deviation above or below mean, respectively, and red color two standard deviations below mean $B_a$. For each $B_a$ the errors from measurements and analytics are added.

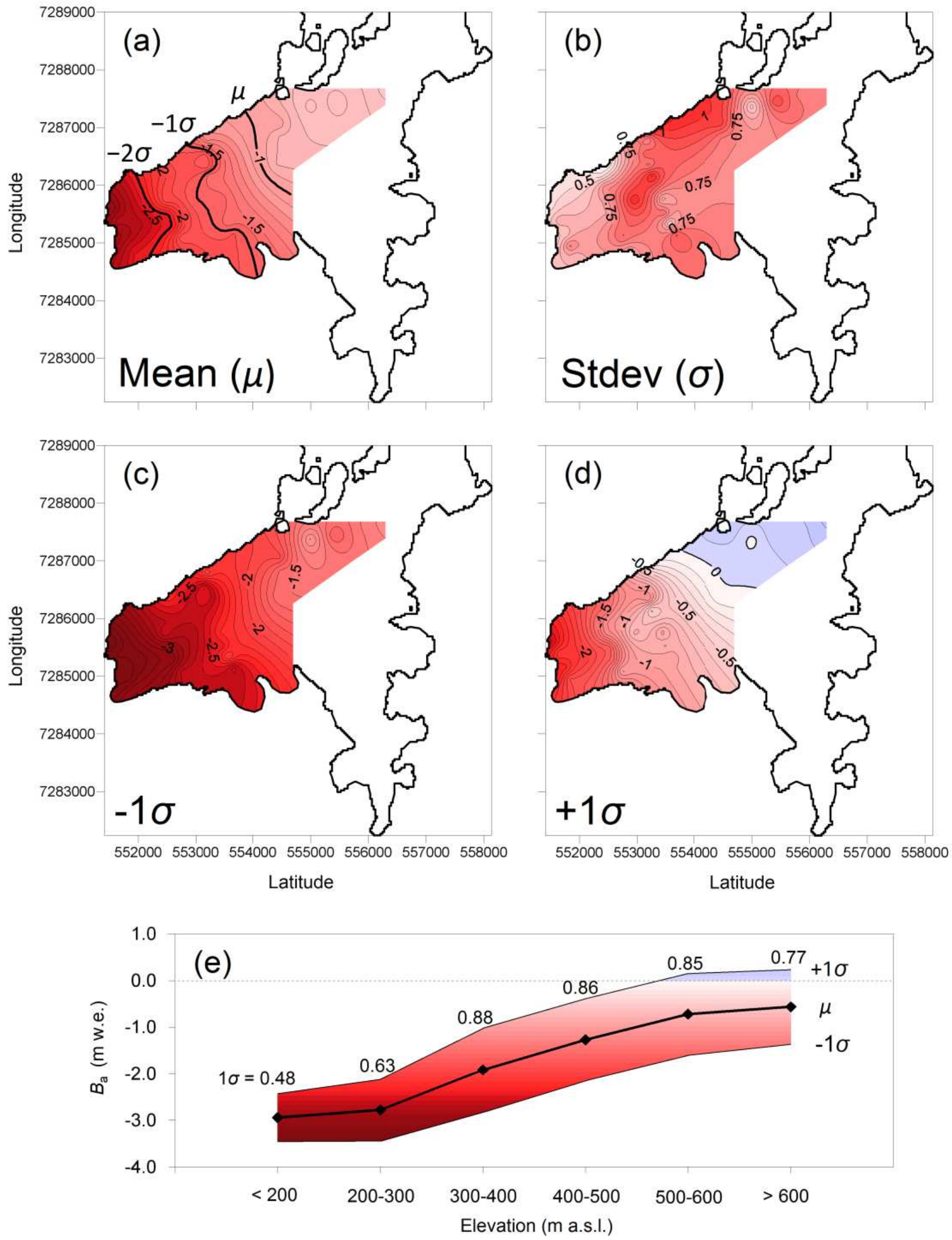


**Figure 6:** Observed Mittivakkat Gletscher (1996/97–2013/14): (a) spatial mean $b_a$ ($\mu$) where one (-1$\sigma$) and two (-2$\sigma$) standard deviations are illustrated with bold lines; (b) spatial distribution of one standard deviation ($\sigma$); (c) spatial $b_a$ minus one standard deviation (-1$\sigma$); (d) spatial $b_a$ plus one standard deviation (+1$\sigma$); and (e) longitudinal $b_a$ profile with plus and minus one standard deviation.

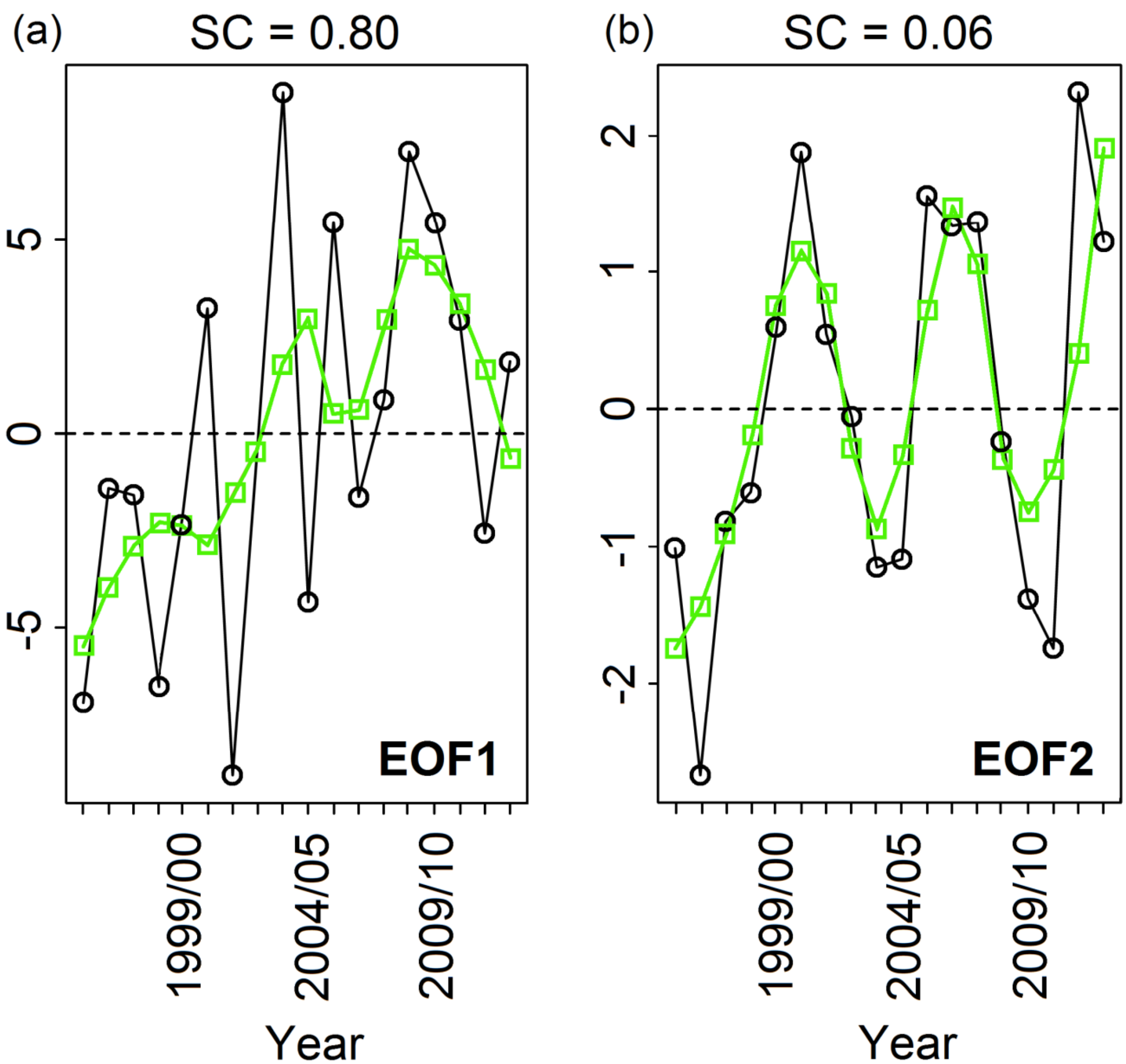


**Figure 7:** Mass-balance time series (1996/97–2013/14) based on the empirical orthogonal functions: (a) EOF1; and (b) EOF2. The explained square covariance (SC) is shown for each EOF. The green line is a five running mean smoothing line.

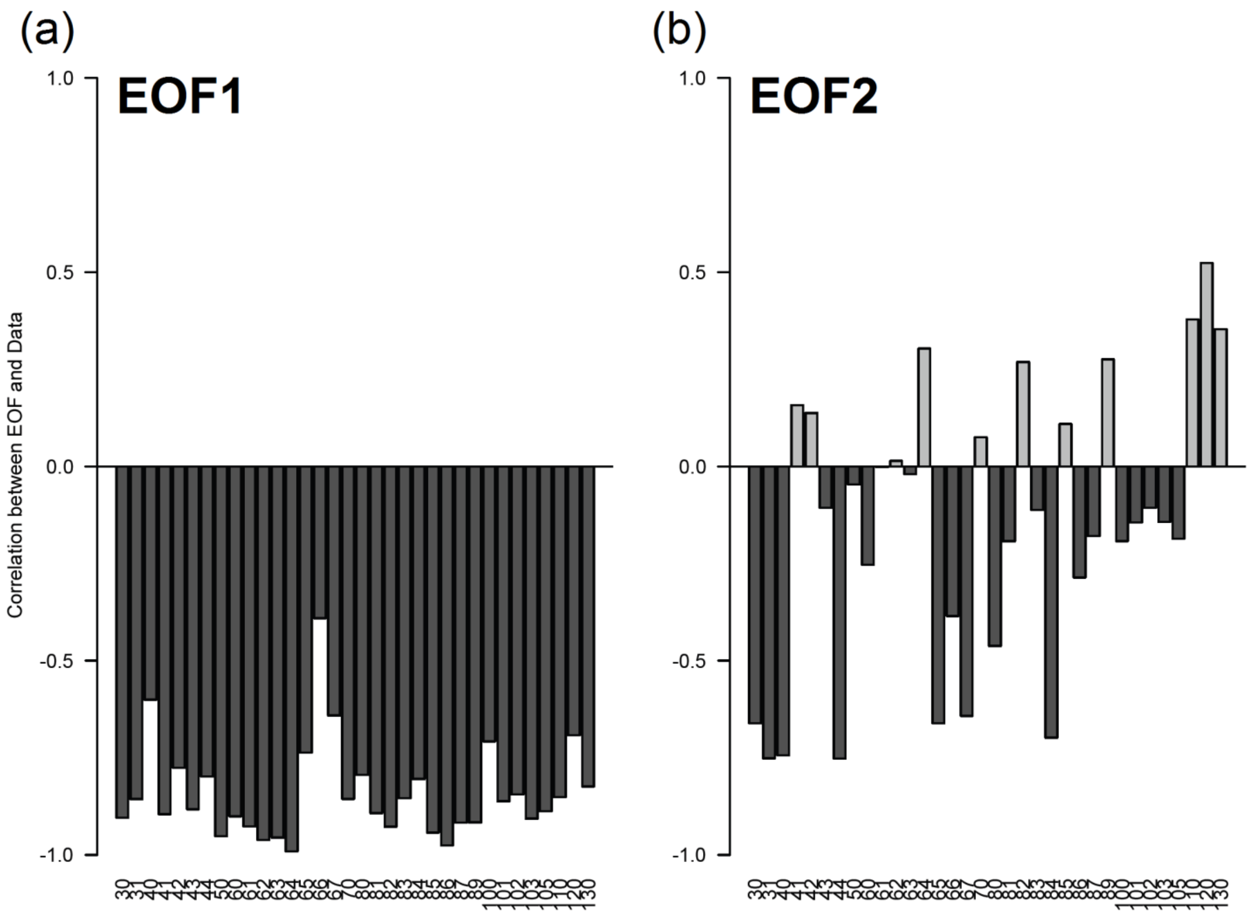


**Figure 8:** Eigenvector correlation values for each individual site for: (a) EOF1, and (b) EOF2. Locations from left to right go from stake 30 to stake 130.

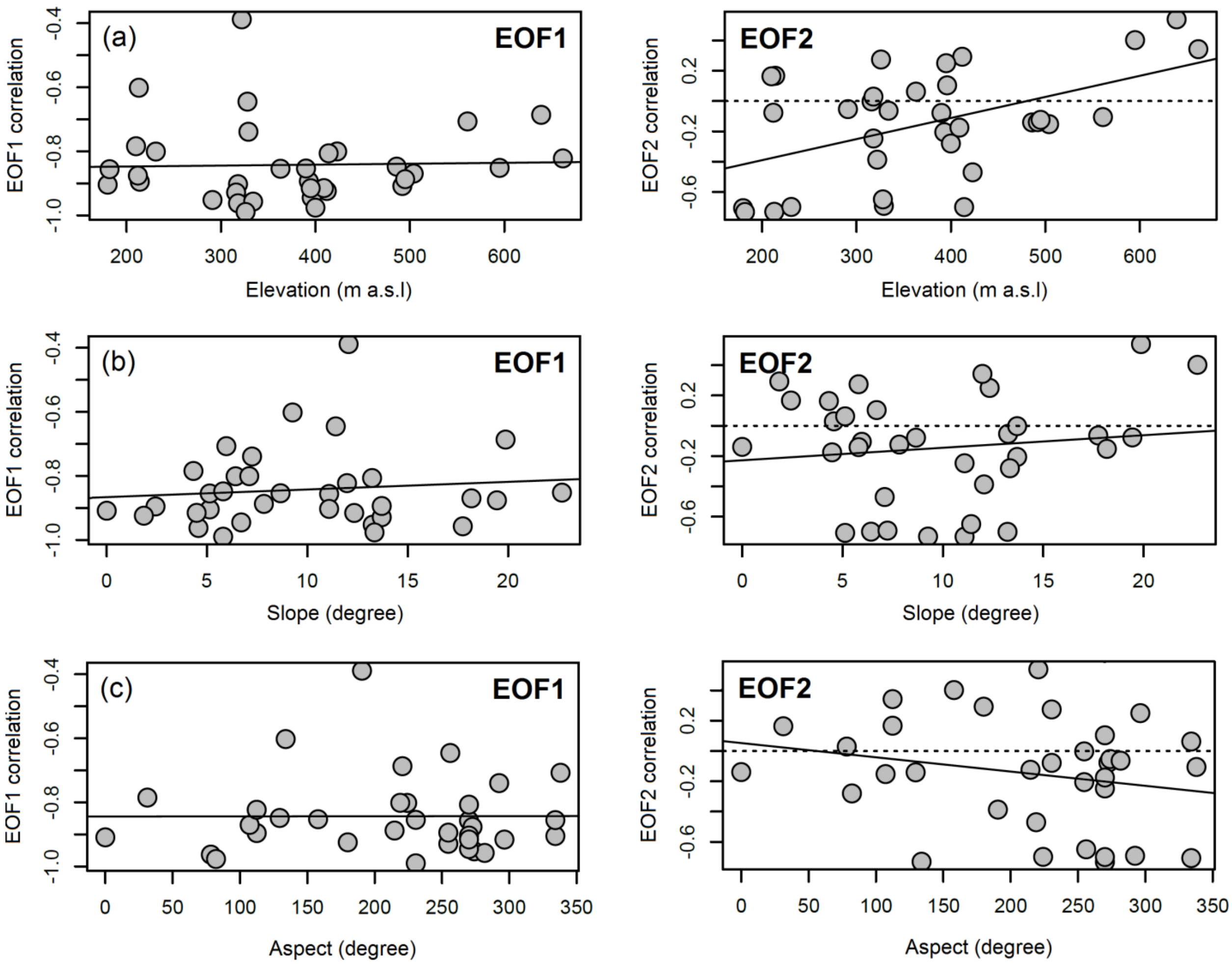


**Figure 9:** EOF1 and EOF2 correlations between: (a) stake elevation; (b) stake surface slope; and (c) stake surface aspect.

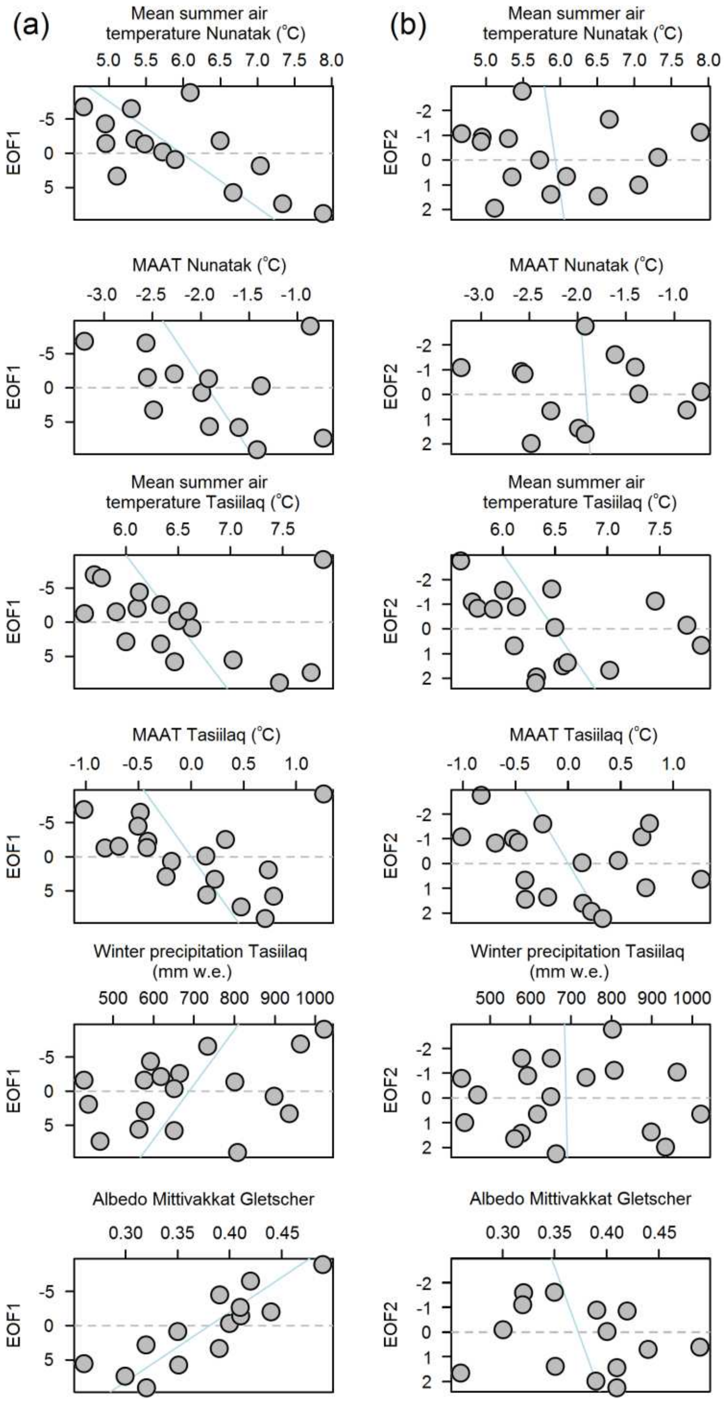


**Figure 10:** (a) EOF1; and (b) EOF2 correlations between Station Nunatak mean summer air temperature, Station Nunatak MAAT, Station Tasiilaq mean summer air temperature, Station Tasiilaq MAAT, Station Tasiilaq winter precipitation, and Mittivakkat Gletscher mean glacier-wide surface albedo by end of the mass-balance year for the 16-days mean period 27/28 July–12/13 August (Mernild et al. 2015b).

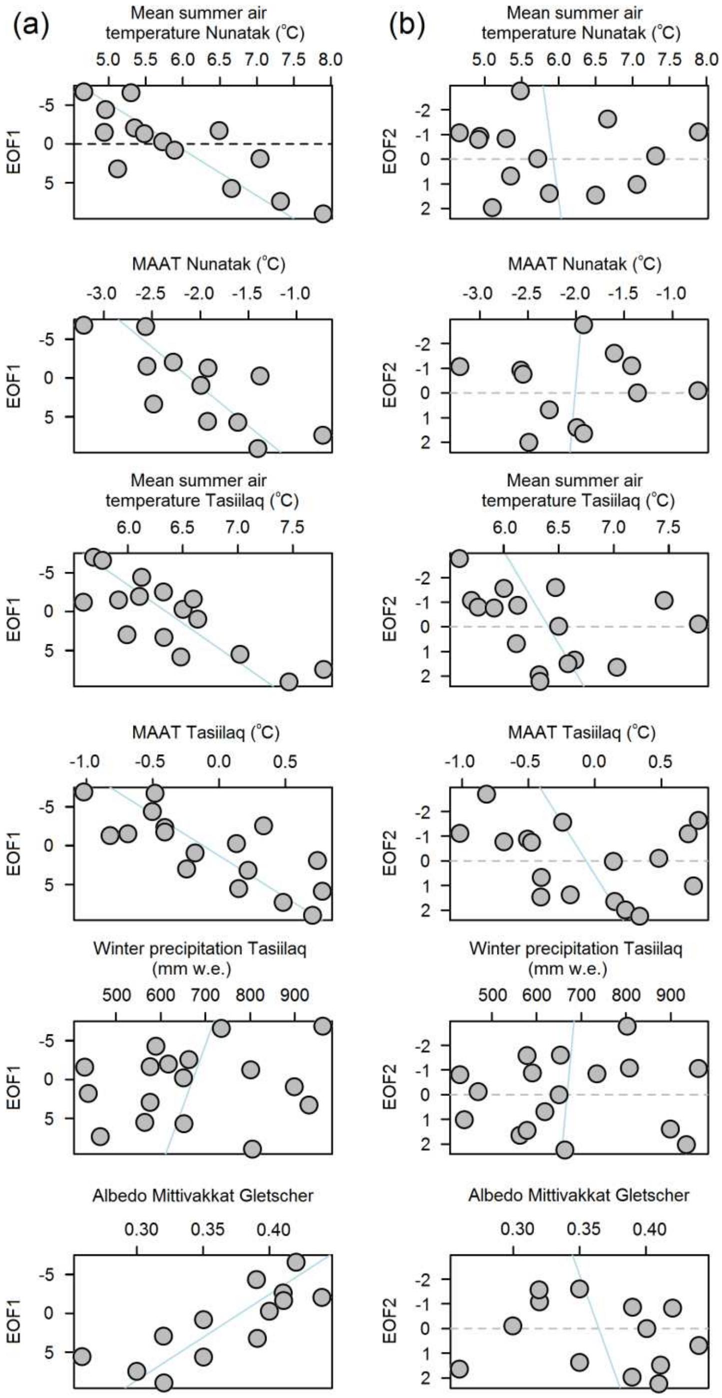


**Figure 11:** (a) EOF1; and EOF2 correlations without the statistical outlier from 2002 between Station Nunatak mean summer air temperature, Station Nunatak MAAT, Station Tasiilaq mean summer air temperature, Station Tasiilaq MAAT, Station Tasiilaq winter precipitation, and Mittivakkat Gletscher mean glacier-wide surface albedo by the end of the mass-balance year for the 16-days mean period 27/18 July–12/13 August (Mernild et al. 2015b).

**Table 1:** Mittivakkat Gletscher surface slope and aspect estimated from ASTER GDEM v2.

| Slope (degrees) | Percentage of area and area | Aspect | Percentage of area and area |
|---|---|---|---|
| 0–5 | 8.3 % (2.2 $km^2$) | North | 11.5 % (3.0 $km^2$) |
| 6–10 | 18.7 % (4.9 $km^2$) | Northeast | 9.8 % (2.6 $km^2$) |
| 11–15 | 20.0 % (5.2 $km^2$) | East | 11.3 % (3.0 $km^2$) |
| 16–20 | 18.2 % (4.8 $km^2$) | Southeast | 8.8 % (2.2 $km^2$) |
| 21–25 | 12.0 % (3.1 $km^2$) | South | 11.2 % (2.9 $km^2$) |
| 26–30 | 8.6 % (2.3 $km^2$) | Southwest | 13.3 % (3.5 $km^2$) |
| 31–35 | 5.6 % (1.4 $km^2$) | West | 19.7 % (5.2 $km^2$) |
| 36–40 | 3.6 % (0.9 $km^2$) | | |
| 41–45 | 2.2 % (0.6 $km^2$) | Northwest | 14.4 % (3.8 $km^2$) |
| >45 | 2.9 % (0.8 $km^2$) | | |

**Table 2:** Statistical relationships between EOF1 and EOF2 and meteorological variables observed near MG and MG mean glacier-wide surface albedo. The lower part of the table is without the statistical outlier from 2002. The letter S = significant, and InS = insignificant.

| All data | | | | | |
|---|---|---|---|---|---|
| | Relationship | Slope | F-value | P-value | $p \leq 0.05$ |
| EOF1 | Mean summer air temperature (Station Nunatak) | 5.98 | 12.37 | 0.00 | S |
| | MAAT (Station Nunatak) | -1.93 | 1.81 | 0.21 | InS |
| | Mean summer air temperature (Station Tasiilaq) | 6.49 | 2.38 | 0.14 | InS |
| | MAAT (Station Tasiilaq) | 0.00 | 2.56 | 0.13 | InS |
| | Winter precipitation sum (Station Tasiilaq) | 688.22 | 2.19 | 0.16 | InS |
| | Mean glacier-wide surface albedo | 0.38 | 32.28 | 0.00 | S |
| EOF2 | Mean summer air temperature (Station Nunatak) | 5.93 | 0.06 | 0.81 | InS |
| | MAAT (Station Nunatak) | -1.92 | 1.94 | 0.18 | InS |
| | Mean summer air temperature (Station Tasiilaq) | 6.49 | 1.94 | 0.18 | InS |
| | MAAT (Station Tasiilaq) | 0.00 | 1.79 | 0.20 | InS |
| | Winter precipitation sum (Station Tasiilaq) | 688.22 | 0.00 | 0.97 | InS |
| | Mean glacier-wide surface albedo | 0.37 | 0.44 | 0.52 | InS |
| All data except the statistical outlier from 2002 | | | | | |
| EOF1 | Mean summer air temperature (Station Nunatak) | 5.88 | 23.11 | 0.00 | S |
| | MAAT (Station Nunatak) | -2.11 | 13.74 | 0.00 | S |
| | Mean summer air temperature (Station Tasiilaq) | 6.35 | 23.59 | 0.00 | S |
| | MAAT (Station Tasiilaq) | -0.12 | 21.63 | 0.00 | S |
| | Winter precipitation sum (Station Tasiilaq) | 672.09 | 0.49 | 0.50 | InS |
| | Mean glacier-wide surface albedo | 0.38 | 19.21 | 0.00 | S |
| EOF2 | Mean summer air temperature (Station Nunatak) | 5.92 | 0.05 | 0.84 | InS |
| | MAAT (Station Nunatak) | -2.01 | 1.64 | 0.22 | InS |
| | Mean summer air temperature (Station Tasiilaq) | 6.41 | 1.64 | 0.22 | InS |
| | MAAT (Station Tasiilaq) | -0.07 | 1.53 | 0.24 | InS |
| | Winter precipitation sum (Station Tasiilaq) | 668.51 | 0.03 | 0.86 | InS |
| | Mean glacier-wide surface albedo | 0.37 | 0.33 | 0.58 | InS |